

CZECH TECHNICAL UNIVERSITY IN PRAGUE
FACULTY OF NUCLEAR SCIENCES AND PHYSICAL
ENGINEERING

Department: Department of Software Engineering
Study programme: Applications of Informatics in Natural science



Modelling laser absorption using machine learning methods

MASTER THESIS

Author: Bc. Samuel Šitina
Supervisor: doc. Ing. Ondřej Klimo, Ph.D.
Year: 2024

ZADÁNÍ BAKALÁŘSKÉ PRÁCE

vložit naskenované zadání, kde jsou všechny podpisy!!!

I. OSOBNÍ A STUDIJNÍ

Příjmení: Jméno: Osobní číslo:
Fakulta/ústav: **Fakulta jaderná a fyzikálně inženýrská**
Zadávací katedra/ústav: **Katedra matematiky**
Studijní program: **(není nutné vyplňovat, doplní se po přepsání do systému)**
Specializace: **(není nutné vyplňovat, doplní se po přepsání do systému)**

II. ÚDAJE K BAKALÁŘSKÉ PRÁCI

Název bakalářské práce:

Název bakalářské práce anglicky:

Pokyny pro vypracování:

1. první bod zadání
2. druhý bod zadání
3. atd.

Seznam doporučené literatury:

- [1] reference č. 1
- [2] reference č. 2
- [3] atd.

Jméno a pracoviště vedoucí(ho) bakalářské práce:

Jméno a pracoviště druhé(ho) vedoucí(ho) nebo konzultanta(ky) bakalářské práce:

Datum zadání bakalářské práce: **bude doplněno** Termín odevzdání bakalářské práce: **bude doplněno**

Platnost zadání bakalářské práce: **bude doplněno**

(jméno vedoucího - bude doplněno)
podpis vedoucí(ho) práce

(jméno vedoucího - bude doplněno)
podpis vedoucí(ho) ústavu/katedry


doc. Ing. Václav Čuba, Ph.D.
podpis děkana

III. PŘEVZETÍ ZADÁNÍ

Student bere na vědomí, že je povinen vypracovat bakalářskou práci samostatně, bez cizí pomoci, s výjimkou poskytnutých konzultací. Seznam použité literatury, jiných pramenů a jmen konzultantů je třeba uvést v bakalářské práci.

Datum převzetí zadání

Podpis studenta



V případě jednostránkového zadání zakomentujte (v *.tex) variantu B1 a odkomentujte např. variantu A1

Statement of originality

Hereby I declare that this thesis is my original authorial work, which I have worked out on my own with the guidance of my supervisor. All sources, references, and literature used or excerpted during the elaboration of this work are properly cited and listed in complete reference to the due source.

In Prague on

.....

Bc. Samuel Šitina

Acknowledgment

I would like to thank my supervisor Doc. Ing. Ondřej Klimo, Ph.D. for valuable guidance throughout the entire process. I would like to thank my parents who have supported unconditionally me in unimaginable ways. I would also like to thank my sister and my brother, whose advice helped me find motivation in the times of struggle.

Huge thanks goes to my friends (yes, even those of you who think plasma is not real), because without you life would be boring and it would be hard to find meaning in anything.

Bc. Samuel Šitina

Title: Modelling laser absorption using machine learning methods

Author: Bc. Samuel Šitina

Study programme: Applications of Informatics in Natural science

Type of thesis: Master thesis

Supervisor: doc. Ing. Ondřej Klimo, Ph.D. Department of plasma physics and fotonics, Faculty of Nuclear Sciences and Physical Engineering, Czech Technical University in Prague

Abstract: Popis práce anglicky

Key words: Klíčová slova

Title:
Modelling laser absorption using machine learning methods

Author: Bc. Samuel Šitina

Abstract: Popis práce česky

Key words: Key words

Contents

Introduction	8
1 Plasma	9
1.1 Temperature of plasma	10
1.2 Ionization	10
1.3 Absorption of ultra-short, ultra-intense lasers	13
1.4 Motivation - X-ray \mathbf{K}_α emission	16
1.5 PIC simulations	18
2 Temperature fitting	22
2.1 Boltzmann vs. Maxwellian distribution	23
2.2 Exponential-sum fitting	24
3 Fitting tool	29
4 Hot electron temperature models	30
5 Hot electron temperature modelling	31
6 Comparison to contemporary data	32
Conclusion	33
Bibliography	34
Attachments	36
A Attachment	36

Introduction

Plasma, the fourth state of matter, constitutes 99% of the visible universe [10].

Chapter 1

Plasma

A plasma is a quasi-neutral gas of charged and neutral particles which exhibits collective behaviour [6]. In simple terms, quasi-neutrality means that the density of electrons n_e and density of positively charged ions n_i locally satisfy:

$$n_e \simeq Z n_i \quad (1.1)$$

where Ze is the charge of one positively charged ion and e is elementary charge [10].

The non-neutral particles in plasma are subject to electric and magnetic fields generated either by external sources or by neighbouring particles. The long-range nature of $1/r$ Coulomb potential ensures that macroscopic fields dominate over forces created by microscopic fluctuations [10]. To explain the collective behaviour properly, one can start by writing *Vlasov equation* [14]:

$$\frac{\partial f_j}{\partial t} + \mathbf{v} \cdot \frac{\partial f_j}{\partial \mathbf{x}} + \frac{q_j}{m_j} \left(\mathbf{E} + \frac{\mathbf{v} \times \mathbf{B}}{c} \right) \cdot \frac{\partial f_j}{\partial \mathbf{v}} = 0 \quad (1.2)$$

where $f_j = f_j(\mathbf{x}, \mathbf{v}, t)$ is the phase space distribution function, which characterizes the location of the particles of species j (electrons or ions) in phase space (\mathbf{x}, \mathbf{v}) (position, velocity) as a function of time. q_j and m_j are charge and mass of the species j and c is the speed of light [14].

After calculating the 0th and 1st moment of Vlasov equation (averaging through \mathbf{v}), we obtain the equation of continuity and force equations for the density $n_j = \int f_j(\mathbf{x}, \mathbf{v}, t) d\mathbf{v}$ and mean velocity \mathbf{u}_j defined by $n_j \mathbf{u}_j = \int \mathbf{v} f_j(\mathbf{x}, \mathbf{v}, t) d\mathbf{v}$:

$$\frac{\partial n_j}{\partial t} + \nabla \cdot (n_j \mathbf{u}_j) = 0 \quad (1.3)$$

$$n_j \left(\frac{\partial \mathbf{u}_j}{\partial t} + (\mathbf{u}_j \cdot \nabla) \mathbf{u}_j \right) = \frac{n_j q_j}{m_j} \left(\mathbf{E} + \frac{\mathbf{u}_j \times \mathbf{B}}{c} \right) - \frac{1}{m_j} \nabla p_j \quad (1.4)$$

where p_j is pressure and in case of negligible heat flow also the energy equation:

$$p_j n_j^{-\gamma} = \text{const.} \quad (1.5)$$

where $\gamma = (2 + N)/N$ and N is the number of degrees of freedom. Equations 1.3, 1.4 and 1.5 together with the Maxwell equations are often referred to as *two-fluid model of plasma* and describe wide range of plasma (collective) behaviour such as plasma waves or Debye shielding [14].

1.1 Temperature of plasma

In this thesis, we are studying so called *hot electrons* produced by the interaction of short laser pulse of high intensity with plasma. All important details of the physical phenomena will be covered in later sections, but let us now look at what is meant by *hot* and how the temperature of plasma is usually understood.

In a gas in the thermal equilibrium, particles can have all velocities usually with Maxwellian distribution (in three dimensions) [6]:

$$f(\mathbf{v}) = n \left(\frac{m}{2\pi k_B} \right)^{3/2} \exp \left(-\frac{\frac{1}{2}mv^2}{k_B T} \right) \quad (1.6)$$

where $v = |\mathbf{v}|$, k_B is the Boltzmann constant and T is temperature. The average kinetic energy E_{av} is then [6]:

$$E_{av} = \frac{3}{2} k_B T \quad (1.7)$$

Because of this relation between E_{av} and T , it is customary in plasma physics to give the temperature the same units as energy. If $k_B T = 1 \text{ eV} = 1.6 \times 10^{-19} \text{ J}$, then [6]:

$$T = \frac{1.6 \times 10^{-19}}{1.38 \times 10^{-23}} = 11600 \quad (1.8)$$

From this it follows that the factor of the conversion is:

$$1 \text{ eV} = 11600 \text{ K} \quad (1.9)$$

The electrons and the ions can have different temperature [6]. What is more, there can be multiple groups of electrons with different distributions, but we will describe this more deeply in one of the later sections.

1.2 Ionization

Any substance can become plasma with the sufficient increase of its temperature. The threshold can vary, but usually can be found in the order of 1 eV, because any neutral atom binds the outer electron with a binding energy in order of 1 eV [23]. The second important factor for ionization is the density of the condensed matter.

Density of plasma

The thermodynamic equilibrium condition for the fraction of electrons $n(\epsilon)$ with energy ϵ is then:

$$n(\epsilon) \propto g(\epsilon) f(\epsilon) \quad (1.10)$$

where $g(\epsilon)$ is the density of state and $f(\epsilon)$ is the Fermi-Dirac distribution (function of T). In the extreme situation of density close to that of a vacuum, found in interstellar space, there are many states for free electrons that escaped from bound

state, and $g(\epsilon)$ is large for free state compared to bound states. For example, for hydrogen atom with given principal quantum number n^* there are $2(n^*)^2$ bound states. This is after the assumption that electron with $n > n^*$ is easily de-trapped. This means that the density of bound states is very low compared to free states and it is for this reason that the interstellar space is assumed to be filled with plasma even though $T \approx 0$ [23].

The examples of plasmas of different densities and temperatures found in the real world can be seen in the table 1.1.

Type	Electron density	Electron temperature
	$n_e \text{ [}(\text{cm})^{-3}\text{]}$	$T_e \text{ [eV]}$
Stars	10^{26}	2×10^3
Laser fusion	10^{25}	3×10^3
Magnetic fusion	10^{15}	10^3
Laser-produced	$10^{18} - 10^{24}$	$10^2 - 10^3$
Discharges	10^{12}	$1 - 10$
Ionosphere	10^6	1.0
Interstellar medium	1	10^{-2}

Table 1.1: Densities and temperatures of various plasma types [10].

Critical density

Now consider a high frequency electric field $\mathbf{E} = \mathbf{E}(\mathbf{x}) \exp(-i\omega t)$. The frequency ω is assumed to be greater than electron plasma frequency ω_{pe} defined as $\omega_{pe}^2 = 4\pi e^2 n_0 / m$ with $n_0 = Zn_{0i}$ being electron density. Maxwell equations give us:

$$\nabla \times \mathbf{B} = -\frac{i\omega}{c}\epsilon\mathbf{E}, \quad (1.11)$$

where $\epsilon = 1 - \omega_{pe}^2 / \omega^2$ defines the dielectric function of the plasma [14]. After further derivation using the other Maxwell equations and vector identities we can get:

$$\nabla^2 \mathbf{B} + \frac{\omega^2}{c^2}\epsilon\mathbf{B} + \frac{1}{\epsilon}\nabla\epsilon \times (\nabla \times \mathbf{B}) = 0 \quad (1.12)$$

Assuming space dependency described by $\exp(i\mathbf{k} \cdot \mathbf{x})$, the dispersion relation is then:

$$\omega^2 = \omega_{pe}^2 + k^2 c^2. \quad (1.13)$$

It is possible to show, that k becomes imaginary for $\omega < \omega_{pe}$. It can be interpreted the following way: electrons shield out the field of a light wave if $\omega < \omega_{pe}$. Because of that, $\omega_{pe} = \omega$ defines the maximum plasma density to which a light wave can penetrate - *critical density*:

$$n_{cr} = \frac{\omega^2 m}{4\pi e^2} = 1.1 \times 10^{21} / \lambda_\mu^2 \text{ cm}^{-3}, \quad (1.14)$$

where λ_μ is the wavelength of the light in microns in vacuum [14].

Ionization mechanisms

There are several mechanisms which can be used to describe ionization. One can start with directly hitting the atoms with fast particles, but for that one would need a stream of such particles. More common way of ionization is achieved by electromagnetic radiation (photoionization) or even via electrical breakdown in strong electric fields [10]. For this thesis, the only relevant ionization is through electromagnetic radiation - in our case a laser.

Firstly, oscillating electromagnetic field makes free electrons oscillate as well and they can ionize other atoms via collisions. New free electrons freed by the collisions can then also hit other atoms and so on.

There are also non-collisional mechanisms of ionization. Imagine field of hydrogen atom at Bohr radius a_B - the most probable distance of electron from the atomic nucleus:

$$a_B = \frac{\hbar}{me^2} = 5.3 \times 10^{-9} \text{ cm} \quad (1.15)$$

where \hbar is the reduced Planck constant, m is the mass of an electron and e is the elementary charge. The electric field for hydrogen E_H is then:

$$E_H = \frac{e}{4\pi\epsilon_0 a_B^2} \simeq 5.1 \times 10^9 \text{ V.m}^{-1}. \quad (1.16)$$

Then the *atomic intensity* for hydrogen I_H is [10]:

$$I_H = \frac{\epsilon_0 c E_H^2}{2} \simeq 3.51 \times 10^{16} \text{ W.cm}^{-2} \quad (1.17)$$

where c is the speed of light in vacuum.

It is reasonable to think that to ionize the hydrogen atom one needs $I_L > I_H$, where I_L is the intensity of the laser. In reality, the ionization occurs already for smaller laser intensities due to so called *multiphoton absorption* [10] and *quantum tunnelling* [23]. The first one can occur, because the electron can climb the virtual energy states one after another and it can get hit by next photon before it falls back to lower energy state [23]. The calculation of these transitions is non-trivial, because one has to solve time-dependant Schroedinger equation. The reader can find deeper analysis in [12].

The tunnelling effect is as well a consequence of the external electric field. The superposition of the electric field which binds the electron to the atom and the strong electric field of the laser results in conditions that allow the electron escape the potential well even if the electron energy is not higher than the threshold energy for instant ionization. Let $V_H(r) = -\frac{C}{r}$ Coulomb potential of hydrogen nucleus, where $C = \frac{e^2}{4\pi\epsilon_0}$. The superposition with strong external field gives us:

$$V_F = V_H(r) + eE_{\text{ext}}(r) \quad (1.18)$$

Let $E_{\text{ext}}(r) = -10^{10}r \text{ V/m}$. The final potential V_F together with highlighted region of tunneling can be seen in figure 1.1.

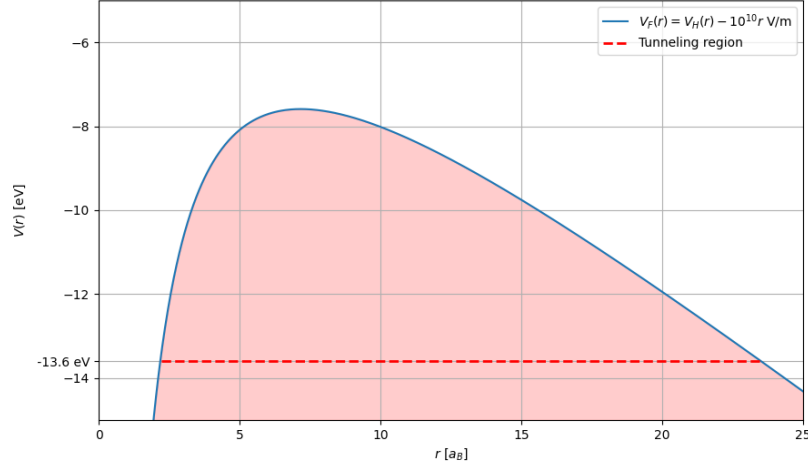


Figure 1.1: The potential of hydrogen atom modified by external field: $E_{\text{ext}} = -10^{10} r \text{ V/m}$. r is shown in radial coordinates with units of Bohr radius a_B . Energy of ground state of electron in hydrogen atom $E_0 = 13.6 \text{ eV}$ is highlighted.

The stronger is the external field, the shorter is the tunnelling distance for the electron to escape. The field can even be so strong that the potential barrier will have its peak below the ground state energy. In that case, the electron is instantly considered to be free [23].

It is possible to estimate, which mechanism is more dominant cause of ionization by calculating so called *Keldysh parameter* $\gamma_K = \frac{\omega_0}{\omega_t}$, where ω_0 is the frequency of the laser and $\omega_t = \frac{eE_{\text{ext}}}{\sqrt{2mE_i}}$, where E_i represents the energy the electron needs to receive to be ionized [23].

The ionization processes can be explored in greater depth, but the fundamental concepts have already been adequately outlined. Henceforth, we will assume the plasma being targeted by the laser is fully ionized and will focus on how it can absorb additional energy from the laser.

1.3 Absorption of ultra-short, ultra-intense lasers

Modern lasers can generate pulses with durations of only few femtoseconds and extremely high intensities (up to $10^{22} \text{ W.cm}^{-2}$) [26], [27]. The interaction of such pulses with dense plasma produces hot electrons [15]. This interaction initiates several processes of energy transfer from the laser's electromagnetic field to the electrons. Let us examine the most significant of these processes.

Collisional absorption

The principles of collisional absorption are similar to those of collisional ionization. In this process, an electron oscillates due to the influence of the laser field and transfers part of its kinetic energy to other ions through collisions. However, since the frequency of ion-electron collisions scales as $\nu_{ie} \propto E^{-3/2}$, this absorption mechanism is primarily significant for laser intensities below $10^{15} \text{ W.cm}^{-2}$ [22]. Given that this thesis focuses on intensities above this threshold, further discussion on collisional absorption is unnecessary.

Resonance absorption

The first non-collisional absorption process we will describe is the *resonance absorption*. This phenomenon can occur during the propagation of a p-polarized light wave through a density gradient. By p-polarized, we refer to a wave that is linearly polarized with its polarization vector lying in the plane of incidence. The complete analytical description is difficult, but after few simplifications it is possible to obtain reasonable idea of the principle [16].

Laser light will reach density $n_t = n_{\text{cr}} \cos^2 \theta$ (from Snell's law [26]), where θ is the angle of incidence [16]. Because of the p-polarization, some light energy will tunnel through the critical density and the electron plasma will be resonantly excited at frequency of the laser ω_0 . The resonant wave is then capable of accelerating electrons and is defined by:

$$\frac{E_d}{\epsilon} = \frac{E_L}{\sqrt{2\pi\omega_0 L_n/c}} \phi(\tau) \quad (1.19)$$

where ϵ is plasma dielectric function, L_n is the density length scale and the parameter $\tau = (\omega_0 L_n/c)^{1/3} \sin \theta$ [26]. It can be approximated that $\phi(\tau) \propto \exp(-2\tau^3/3)$ [16]. Deeper derivation of the equation 1.19 can be found in [16] starting on page 139.

The angle of optimum resonance absorption for exponential density profile θ_{opt} can then be estimated as a function of L :

$$\theta_{\text{opt}}(L) = \arcsin(0.68(2\pi L)) \quad (1.20)$$

where L is normalized to the laser wavelength [22].

Vacuum heating

The second non-collisional absorption process (and no less important than the first one) is called *Vacuum heating* or sometimes *Brunel effect* or even “*not-so-resonant*” *resonance absorption* [4]. It was proposed by Mr. Brunel in 1987 it was later confirmed by many experiments [26].

Like before, p-polarized laser pulse is needed. At the angle of incidence θ the laser is hitting the target with steep density profile (a big gradient). A part of the pulse is refracted and a part is reflected. The incoming laser wave \mathbf{E}_L and reflected wave

\mathbf{E}_R are in superposition at point of incidence $x = 0$ and the resulting field has a perpendicular component with amplitude $E_0 = 2E_L \sin \theta$, under approximation that $E_L = E_R$. Poisson's equation at the surface gives us [26]:

$$\Delta E = -4\pi e \int_{x=-\Delta x}^{x=0} n dx = 4\pi e n \Delta x. \quad (1.21)$$

The electrons are pulled out from plasma by that field according to the equation 1.21. If $n = N/(A\Delta x)$ with N/A being number of electrons pulled out into vacuum per unit area and if $\Delta E = E_0$, we get [26]:

$$\frac{N}{A} = \frac{2E_0 \sin \theta}{4\pi e}. \quad (1.22)$$

The energy absorbed E_{abs} by the electrons is then [26]:

$$E_{\text{abs}} = \frac{1}{2} N m_e v_e^2. \quad (1.23)$$

After calculating the power absorbed by unit area and after substituting v_0 with *quiver velocity* v_{osc} defined by: $\frac{v_{\text{osc}}}{c} = \frac{eE_0}{m_e c \omega_0}$, we get the absorbed fraction of the power $f_{\text{VH}} = I_{\text{abs}}/I_0$ [26]:

$$f_{\text{VH}} = 8 \frac{v_{\text{osc}}}{c} \sin^3 \theta \quad (1.24)$$

Note that we made a simplification by letting $E_L = E_R$. Another option would be to directly write $E_0 = (1 + R^{1/2}) E_L \sin \theta$, where R is the reflectivity [22]. We also neglected that the electron in vacuum is very fast and therefore relativistic correction has to be made. It is possible to generally follow a more rigorous path found for example in [15] and [22]. Then the formula for f_{VH} is expanded to:

$$f_{\text{VH}} = \frac{\eta}{2\pi} \frac{1}{a_0} \frac{\sin \theta}{\cos \theta} (1 + R^{1/2}) \left\{ \left[1 + (1 + R^{1/2})^2 a_0^2 \sin^2 \theta \right]^{1/2} - 1 \right\}, \quad (1.25)$$

where $\eta = 1.74$ and $a_0 = eE_L/(m_e \omega_0 c)$.

$\mathbf{J} \times \mathbf{B}$ heating

The last absorption mechanism we want to discuss is usually called *$\mathbf{J} \times \mathbf{B}$ heating*. In the sections above, we discussed the heating of plasma due to electron motion in the direction of the oscillating \mathbf{E} component of the laser beam. That is of course caused by the $e\mathbf{E}$ part of the Lorentz force. The other part - $\mathbf{j} \times \mathbf{B}$ - can be neglected in non-relativistic cases. However, for laser intensities higher than $10^{17} \text{ W.cm}^{-2}$ it is not possible to explain all absorption using the classical limit and another consideration has to be made [5].

Let ϕ and \mathbf{A} be scalar and vector potential ($\mathbf{E} = -\nabla\phi$ and $\mathbf{B} = \nabla \times \mathbf{A}$) satisfying Coulomb gauge $\nabla \cdot \mathbf{A} = 0$. Also, we can separate transverse and longitudinal part of electron momentum $\mathbf{p} = \mathbf{p}_t + \mathbf{p}_l$. Then the equations of motion for electron can be written as [5]:

$$\frac{\partial \mathbf{p}_t}{\partial t} = \frac{e}{c} \frac{\partial \mathbf{A}}{\partial t} \quad (1.26)$$

$$\frac{\partial \mathbf{p}_l}{\partial t} = e \nabla \phi - m_e c^2 \nabla (\gamma - 1) \quad (1.27)$$

where $\gamma = \sqrt{1 + \frac{p_{osc}^2}{2m_e^2 c^2}}$ is the relativistic factor for linearly polarized light [26]. The second term of the equation 1.27 is the relativistic ponderomotive force and we can write the ponderomotive potential U_p as:

$$U_p = m_e c^2 \nabla (1 - \gamma). \quad (1.28)$$

After expanding γ as a fourier series with frequency ω_0 :

$$\gamma(z, t) = \gamma_0(z) + \gamma_1(z) e^{i\omega_0 t} + \gamma_2(z) e^{i2\omega_0 t} + \dots \quad (1.29)$$

we get $\gamma_1 = 0$ and $\gamma_2 \approx a_1^2/4$, where a_1 is defined with:

$$\mathbf{a}(z, t) = e \mathbf{A}(z, t) / m_e c^2 = \hat{\mathbf{x}} \frac{1}{2} [a_1(z) e^{i\omega_0 t} + \dots] \quad (1.30)$$

where $\hat{\mathbf{x}}$ is a unit vector in the x direction [5].

Thanks to the expansion, it is clear that there is a force with frequency $2\omega_0$ which will affect the electrons in longitudinal direction. One of the interpretations of this force can sound like this: Twice every laser period, streams of electrons are pushed into the target [5]. This causes energy transfer to the rest of the plasma resulting in the production of fast electrons.

It is important to note, that at higher intensity, the electron density can rise as a consequence of the zero-frequency ponderomotive force. The change in density can cause that the $2\omega_0$ resonance is not possible. The density is also dependent on the scale length of the target. For example for exponential density profile, the density decreases with the increase of scale length [5]. This means the $2\omega_0$ resonance is expected to play a greater role for bigger scale lengths. In other words, the initial plasma conditions need to be known to estimate the effects of $\mathbf{J} \times \mathbf{B}$ heating.

One last note regarding $\mathbf{J} \times \mathbf{B}$ heating. The relativistic factor γ has a different form in a case of circularly polarized laser. That leads to suppressing this kind of electron heating altogether [5].

Last words on absorption

The three mentioned mechanisms are by no means exhaustive when it comes to laser absorption. They are the three most relevant in the context of this work. There are other physical contributing to heating up the plasma especially when the parameters of the experiment change [22]. We will now move on to motivating the thesis in greater detail.

1.4 Motivation - X-ray K_α emission

Because hot electrons accelerated by ultra-intense ultra-short laser pulse can carry multi-keV energy, they can penetrate a solid behind the plasma, where by K -shell

ionization they can generate X-rays [19]. The X-ray is consisting of spectral lines (K_α) and X-ray from Bremsstrahlung. The uniqueness of this method are the high energies of monochromatic photons within a short pulse synchronized with the laser pulse. The source is typically very small [18].

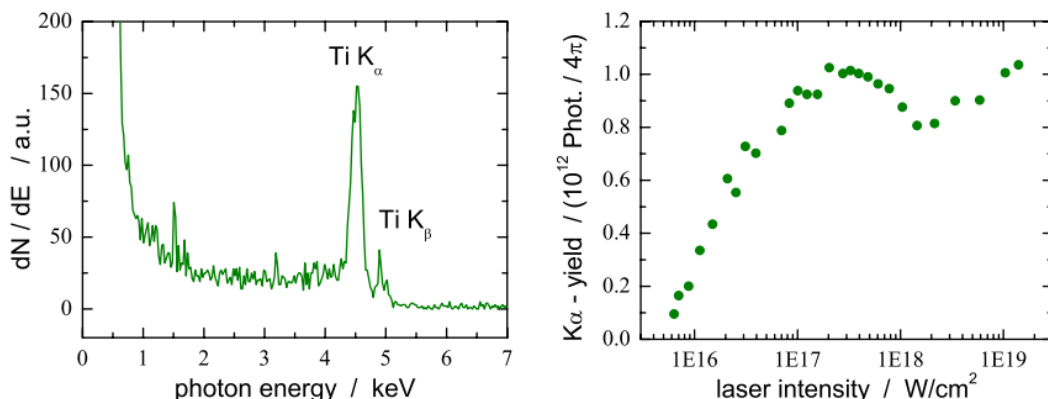


Figure 1.2: *Left:* The spectrum of laser generated K_α and K_β radiation of titanium. *Right:* The scaling of K_α - yield in relation to laser intensity. [21]

Let us now briefly look into the origin K_α -line. In figure 1.2, there is a spectrum of titanium for x-ray photon energies and how the K_α - yield scales with the laser intensity. The generation of the K_α radiation clearly depends on laser intensity and therefore in some sense also on hot electrons temperature. According to [21], the yield drops at the laser intensity around $10^{18} \text{ W.cm}^{-2}$ *"because the interaction time with the atom decreases with higher electron velocity"*. The following rise in the yield is then attributed to the relativistic effect where the electric fields of the fast hot electrons are contracted and therefore have greater effect [21].

The total yield N can be expressed analytically as [19]:

$$N = \int n_{\text{hot}} f_{\text{hot}}(E) N_{\text{gen}}(E) f_{\text{em}}(E) dE \quad (1.31)$$

where N is the number of emitted photons, n_{hot} is the total number of hot electrons, and $f_{\text{hot}}(E)$ is their energy distribution, $N_{\text{gen}}(E)$ is the number of K_α photons generated by an electron of incidence energy E , and $f_{\text{em}}(E)$ is the fraction of these photons that escapes from the solid [19].

Having a reliable numerical model of n_{hot} and $f_{\text{hot}}(E)$ from equation 1.31 could allow us to optimize the K_α yield based on the parameters of the laser and the plasma. Namely, the angle of incidence, the laser intensity and the plasma length scale. The research conducted by Reich et al. [19] could be followed up by examining a wider range of parameters beyond just laser intensity. This is crucial because, as shown by Cui et al. [7], the temperature function of the electrons has a complex and non-trivial shape. The complexity comes from the complex nature of the physical processes causing the electron heating.

In this thesis, we presents results from hundreds of PIC simulations while scanning through the mentioned parameters. Then we try to present and defend a way of

how the hot electron temperature can be modelled and how to make the model more precise. The implications with respect to previous works and to equation 1.31 are discussed.

1.5 PIC simulations

As previously mentioned, we are using Particle-In-Cell (PIC) simulations to obtain the data necessary for our model. PIC codes have been under development since the advent of computers in the 1960s, and advancements in computer technology over the past 30 years have enabled us to run simulations on a much larger scale. One significant advantage of simulations is that they allow theoretical predictions to be verified in greater detail than is possible with real plasma experiments [8]. To illustrate the progress made over the decades, let us mention, that in 1962 Dawson and Buneman simulated the motion of 1000 plasma particles. Today, we can simulate the motion of more than 10^{10} particles [24].

We are not developing our own simulation code. Instead, we are using code freely available for academic purposes, specifically the 2D simulation code EPOCH [1]. EPOCH has been widely used in numerous publications within the laser-plasma field and adequately meets our requirements. Below, we will present a brief overview of the key principles of the PIC method, upon which EPOCH is also based.

Macro-particles

It is not possible to have as many particles in a simulation as in a real plasma, even in very small scales, because of the computational cost. Because of that, the simulations usually work with macro-particles which represent clouds of many real particles. These particles have finite sizes (as opposed to infinitesimal), so that there are no divergent forces in case of collisions. The forces in simulations go to zero for small distances between macro-particles. For large distances, they comply with the Coulombic behaviour. In plasma simulations, it is possible to do this without sacrificing accuracy, because of the collective behaviour of plasma[20].

Computational cycle

The simulation runs in a cycle. In each step, we solve for electromagnetic fields created by the charged particles. Then we evaluate the equations of motion for the particles, which are influenced by the Lorentz force [3]. The laser pulse is included as an external source of electromagnetic radiation at the boundary.

Typically, the finite-difference time-domain method (FDTD) is used for numerically solving Maxwell's equations, which fully describe the electromagnetic field. *Finite-difference* means that the electric field \mathbf{E} and magnetic field \mathbf{B} are specified in the points of a grid - usually a *Yee grid*. A comprehensive description of a Yee grid can be found in the original article by Yee [28]. The critical concept of a Yee grid

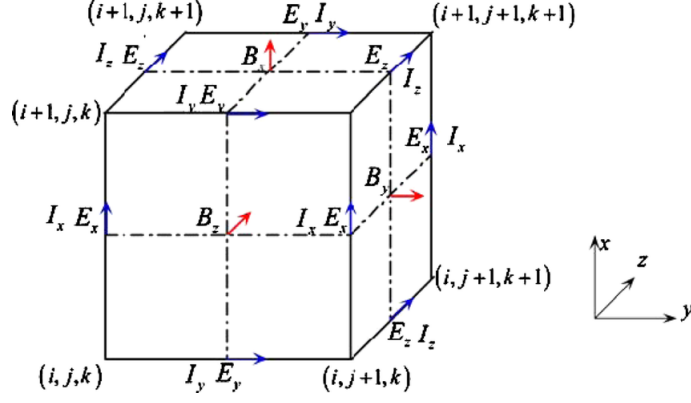


Figure 1.3: An illustration of a Yee grid [25]

is illustrated in figure 1.3. - the magnetic field components are calculated in the center of the faces of an imaginary cube (cell) while the electric field components are calculated in the center of the edges. The cube represents one cell of the 3-dimensional grid. We can write derivatives of electric field [1]:

$$\left(\frac{\partial E_y}{\partial x}\right)_{i+\frac{1}{2},j,k} = \frac{E_{y,i+1,j,k} - E_{y,i,j,k}}{\Delta x} \quad (1.32)$$

Note, that this numerical derivative in equation 1.32 is second order accurate at the cube point where we calculate $B_{z,i,j,k}$, because the formula is centered. Moreover, because of one of the Maxwell's equations, $\nabla \times \mathbf{E} = \frac{\partial \mathbf{B}}{\partial t}$, this derivative is exclusively used to calculate time-derivative of $B_{z,i,j,k}$. A similar relationship can be found when calculating all components of \mathbf{B} from \mathbf{E} and vice versa. Therefore, all used numerical derivatives are second order accurate [1].

In EPOCH, as in other PIC codes, fields are updated at both the half time-step and full time-step. The first part - time-step from n to $n+1/2$ - uses currents calculated at n :

$$\mathbf{E}^{n+1/2} = \mathbf{E}^n + \frac{\Delta t}{2} \left(c^2 \nabla \times \mathbf{B}^n - \frac{\mathbf{J}^n}{\epsilon_0} \right) \quad (1.33)$$

$$\mathbf{B}^{n+1/2} = \mathbf{B}^n - \frac{\Delta t}{2} (\nabla \times \mathbf{E}^{n+1/2}) \quad (1.34)$$

where \mathbf{J} is the current density and Δt is a size of a full time-step [1].

In the second step, with updated currents, we use the current extrapolated to step $n+1$:

$$\mathbf{B}^{n+1} = \mathbf{B}^{n+1/2} - \frac{\Delta t}{2} (\nabla \times \mathbf{E}^{n+1/2}) \quad (1.35)$$

$$\mathbf{E}^{n+1} = \mathbf{E}^{n+1/2} + \frac{\Delta t}{2} \left(c^2 \nabla \times \mathbf{B}^{n+1} - \frac{\mathbf{J}^{n+1}}{\epsilon_0} \right) \quad (1.36)$$

The motion of particles and the resulting currents are consequences of these fields. Generally, the equations of motion are:

$$\frac{d\mathbf{x}_l}{dt} = \mathbf{v}_l \text{ and } \frac{d\mathbf{p}_l}{dt} = \mathbf{F}_l \quad (1.37)$$

where vectors \mathbf{x}_l , \mathbf{v}_l and \mathbf{p}_l represent the position, velocity and momentum of the l -th macro-particle. $\mathbf{F}_l = \mathbf{F}_l(t, \mathbf{x}_l, \mathbf{v}_l, \mathbf{E}, \mathbf{B})$ is the force. Fields \mathbf{E} and \mathbf{B} are functions of the positions and velocities of the all charged particles [24]. In this context, the right-hand side of the second equation represents the Lorentz force, and the time-step formula for the momentum is: [1]:

$$\mathbf{p}_l^{n+1} = \mathbf{p}_l^n + q_l \Delta t \left[\mathbf{E}^{n+1/2}(\mathbf{x}_l^{n+1/2}) + \mathbf{v}_l^{n+1/2} \times \mathbf{B}^{n+1/2}(\mathbf{x}_l^{n+1/2}) \right] \quad (1.38)$$

where q_l is the charge of the l -th particle. The velocity can be calculated from the momentum using:

$$\mathbf{v}_l = \frac{\mathbf{p}_l}{\gamma_l m_l} \quad (1.39)$$

where m_l is the mass of the particle and $\gamma_l = [p_l^2/(m_l^2 c^2) + 1]^{1/2}$ is the corresponding gamma-factor [1].

The particle position update is calculated from the velocity, but this is also done in multiple steps. First, we calculate movement of half time-step from the old velocity as we need it to update the momentum in equation 1.38 [1]:

$$\mathbf{x}_l^{n+1/2} = \mathbf{x}_l^n + \frac{\Delta t}{2} \mathbf{v}_l^n \quad (1.40)$$

In similar way, we can then calculate \mathbf{x}_l^{n+1} and $\mathbf{x}_l^{n+3/2}$ [1], which are needed for calculating the currents.

The currents necessary for updating the fields can be calculated using methods such as the one presented by Esirkepov in [9]. Modern approaches to calculating currents are generally based on solving the continuity equation:

$$\frac{\partial \rho}{\partial t} + \nabla \cdot \mathbf{J} = 0 \quad (1.41)$$

where ρ is the charge density and \mathbf{J} is the electric current. This can be discretized as:

$$\frac{\rho_{i+1/2,j+1/2,k+1/2}^{n+1} - \rho_{i+1/2,j+1/2,k+1/2}^n}{\Delta t} + \frac{J_{x,i+1,j+1/2,k+1/2}^{n+1/2} - J_{x,i,j+1/2,k+1/2}^{n+1/2}}{\Delta x} + \dots = 0. \quad (1.42)$$

The charge density is calculated using *form-factors* of macro-particles:

$$\rho_{i,j,k} = \sum_l Q_l S_{i,j,k}(x_l, y_l, z_l) \quad (1.43)$$

where Q_l is the charge and $S_{i,j,k}(x_l, y_l, z_l)$ is the form-factor. During macro-particle motion, the total charge should remain constant, necessitating that the form-factors satisfy the condition :

$$\sum_{i,j,k} S_{i,j,k}(x_l, y_l, z_l) = 1 \quad (1.44)$$

Since macro-particles in the simulation represent numerous real particles, a *weight* is assigned to each macro-particle. Although the exact particle distribution within

a macro-particle is unknown, a representative function, known as a *shape function*, is chosen.[1].

Any function with a unit integral and compact support can be used as a shape function. An even distribution of particle in volume $\Delta x \times \Delta y \times \Delta z$ is referred to as the *top hat* shape function. Using higher order shape functions are one of the improvements programmers were able to make thanks to more powerful computers. A higher order shape functions are for example triangular shape functions with volume of $2\Delta x \times 2\Delta y \times 2\Delta z$. The weight is then calculated as a convolution of shape function with the 'top hat' function [1].

Working with macro-particles instead of individual particles neglects some effects, particularly those effective over distances shorter than Δx . EPOCH uses a fully relativistic, energy-conserving binary collision model, which favors small-angle scattering to improve simulation behavior with a limited number of particles per cell. For our study involving laser intensities above 10^{10} , collisions are not necessary. Other effects, such as ionization and quantum phenomena like photon emission and pair production, are often included when relevant, with detailed descriptions available in [1].

Chapter 2

Temperature fitting

The results of the EPOCH simulations provide weighted momenta of electrons \mathbf{p}_e , where the weight represents the number of electrons with that momentum. They are not histograms yet, because more than one macro-particle can be assigned with the same value of \mathbf{p}_e . The energies of electrons can then be calculated from \mathbf{p} using the relativistic formula:

$$E_e = m_0 \cdot c^2 \left(\sqrt{1 + \left(\frac{p}{m_0 \cdot c} \right)^2} - 1 \right), \quad (2.1)$$

where $p = \sqrt{\mathbf{p} \cdot \mathbf{p}}$ is the size of \mathbf{p} , $m_0 = 9.109 \times 10^{-31}$ kg is the electron rest-mass and $c = 3 \times 10^8$ m.s⁻¹ is the speed of light **cite-the-constants**.

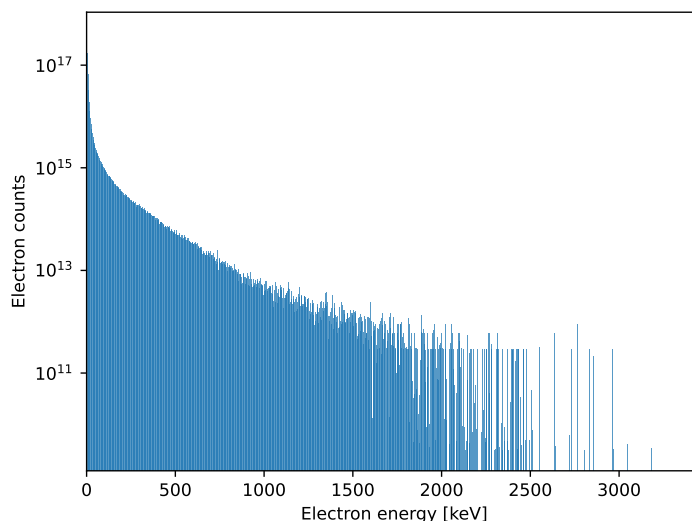


Figure 2.1: An example of electron energy distribution of 2D EPOCH simulation with intensity of laser $I = 10^{19}$ W.cm⁻², characteristic scale of the exponential preplasma profile $L = 0.1$ μ m and angle of incidence with respect to target normal direction $\alpha = 10^\circ$.

After using equation 2.1 to calculate energy, it is multiplied by the weight. One can then easily create the histogram from electron energies and their counts. An example of such histogram can be seen in the figure 2.1. There are several things that need to be discussed.

Firstly, it is important to note that the y -axis is presented on a logarithmic scale to enhance readability. The extensive range of electron energies necessitates the use of relativistic formula. However, around the energies $E_k \approx 1900 \text{ keV}$ and more, the histogram exhibits irregularities - specifically, there are empty bins and several bins contain identical electron counts. These anomalies are attributed to the EPOCH weighting process. Consequently, this portion of the spectrum is rendered questionable. This issue will be further addressed in the section dedicated to temperature fitting.

Last but not least, note the apparent exponential relationship between N_i and E_k in the energy spectrum between $E_k \approx 500 \text{ keV}$ and $E_k \approx 1500 \text{ keV}$:

$$N_i = N_0 \cdot \exp\left(-\frac{E_i}{T}\right), \quad (2.2)$$

where N_i is count in i -th bin and E_i is the corresponding energy and T is temperature in units discussed in section 1.1. The relationship is, of course, linear after the logarithmic transformation. The equation of 2.2 resembles exponential distribution with $1/T$ missing on the right-hand side. It is also not normalized, because it represents counts that have to add up to total number of electrons with that temperature. For the purpose of this thesis, we will call it the *Boltzmann distribution*, even though it is not completely accurate.

Fitting the correct part of the histogram using equation 2.2 and estimating T and N_0 is the first bigger part of this thesis. There are several obstacles, all of which are discussed in following sections.

2.1 Boltzmann vs. Maxwellian distribution

First of all, in section 1.1, where we introduced temperature as a quantity describing plasma, we said that the distribution of energies is usually considered to be Maxwellian. The question, whether we can fit our histogram using Boltzmann distribution, is therefore valid and needs to be addressed.

The equations for the Maxwellian $f_M(E)$ and Boltzmann $f_B(E)$ distributions can be after few simplifications regarding units defined as:

$$f_M(E)dE = \frac{1}{(ET)^{3/2}} \exp\left(-\frac{E}{T}\right) dE \quad (2.3)$$

and

$$f_B(E)dE = \frac{1}{T} \exp\left(-\frac{E}{T}\right) dE. \quad (2.4)$$

By ignoring that both are defined by the differential, taking logarithm of both $f_M(E)$ and $f_B(E)$ we get:

$$\bar{f}_M(E) = \log(f_M(E)) = \log\left(\frac{1}{(ET)^{3/2}}\right) + \left(-\frac{E}{T}\right) \quad (2.5)$$

and

$$\bar{f}_B(E) = \log(f_B(E)) = \log\left(\frac{1}{T}\right) + \left(-\frac{E}{T}\right). \quad (2.6)$$

These two equations describe the distributions in a logarithmic scale. The first derivatives are then:

$$\frac{d\bar{f}_M}{dE} = -\frac{3}{2} \frac{(ET)^{3/2}}{(ET)^{5/2}} - \frac{1}{T} = -\frac{3}{2} \frac{1}{ET} - \frac{1}{T} = -\frac{1}{T} \left(1 + \frac{3}{2E}\right) \quad (2.7)$$

and

$$\frac{d\bar{f}_B}{dE} = -\frac{1}{T}. \quad (2.8)$$

The equations 2.7 and 2.8 suggest that in the logarithmic scale the slopes of these distributions differ by $-\frac{3}{2} \frac{1}{ET}$, which decreases with increasing E . In other words, the fit of T can be replaced by fitting slope $s = -1/T$ of the histogram after logarithmic transformation. For large energies, the slopes of both discussed distributions are approximately equal. The formula for Maxwellian distribution changes when working with momentum in 2 dimensions, but it can easily be shown that the conclusion is not affected.

What is more, the assumption of Boltzmann distribution allows us to fit not only the temperature, but also N_0 , which is the total number of electrons in that distribution of hot electrons. If we keep the form of the distribution as in equation 2.2, the total energy absorbed by the group of hot electrons E_{tothot} with temperature T_{hot} can be calculated as:

$$E_{\text{tothot}} = N_0 \cdot T_{\text{hot}}^2. \quad (2.9)$$

2.2 Exponential-sum fitting

Exponential-sum fitting has been a recognized challenge for many years. Forman S. Acton, a professor at Princeton University, addressed this issue in his 1970 book Numerical Methods That Work. Among various topics, he included an essay titled "What Not to Compute," wherein he described the fitting of sums of exponential functions as "extremely ill-conditioned" **acton**. Despite the inherent difficulty of this problem, this thesis endeavors to determine electron temperatures, necessitating the development of an effective solution to this challenging computational task.

The task is to find the parameters $m, a_0, a_1, \dots, a_m, b_1, \dots, b_m$ so that the function

$$f(x) = a_0 + \sum_{i=1}^m a_i e^{b_i x} \quad (2.10)$$

generalizes the data as good as possible. Formally, for a set of data (n data points) $((x_1, y_1), \dots, (x_n, y_n))$ we are minimizing error function

$$e = \sum_{i=1}^n w_i (y_i - f(x_i))^2 \quad (2.11)$$

where w_i are the weights.

Modern programming libraries provide access to well-known and generally efficient methods, such as non-linear least squares. However, due to the previously mentioned ill-conditioning, these methods do not yield satisfactory results in this context. The convergence of these methods is highly dependent on the quality of the initial guess, which poses a significant challenge. To date, significant efforts have been made to develop reliable methods for solving this problem.

Notably, Prony’s method **prony** and its variations, as discussed in sources such as **prony2**, have been proposed. It was originally intended for signal approximation - specifically, the determination of complex parameters in exponential functions, similar to Fourier transformation.

Another, much simpler method is known as *successive subtraction* **fitexp-trans**. This method is frequently employed for exponential decays (negative parameters b_i), which closely resemble our problem of exponential distributions. The core concept involves fitting the end of the decay with a single exponential function, subtracting this result from the data, and iteratively identifying all exponential components. This simplicity makes it a promising candidate for our problem, especially since our primary interest lies in determining the temperature of the hottest electrons—the tail. However, automating this method can be challenging, as it is not straightforward to select an interval that can be fitted as a tail in each iteration. What is more, the tail of our histograms are not reliable as was discussed with regard of the example histogram in figure 2.1.

Another method worth considering is presented in **fitexp-trans**. This method, called exponential sum fitting of transmissions (ESFT), was developed for fitting radiative transmission functions in the context of atmospheric research. ESFT too is an iterative method and might serve as an interesting alternative for future works.

We only mentioned a few methods. A summary with a deeper explanation of these and other methods can be found in **fitexp-trans**, **fitexp-summary** or in **fitexp-summary2**.

If the goal is to fit only one of the exponentials, such as the parameters of the hot electrons distribution, the standard approach involves manually selecting the “correct” segment of the distribution and fitting it with a single exponential function. For instance, in [7], where researchers study a problem similar to ours, they appear to use this technique to determine the temperature of hot electrons. The term “correct” is somewhat vague because it can be subjective and we do not have any metric that would quantify how well the segment was chosen. We can only work with the metrics describing the fit itself.

The last mentioned option currently provides the most reliable approach to fitting the temperature of hot electrons. Even for hundreds of simulations, with the right tool, it is possible to fit manually every histogram within few hours. Having such dataset of histograms and temperatures is valuable for evaluating any method that is trying to automate the fitting process. A tool with an UI was developed specifically for this purpose as a part of this work.

That being said, we still attempted to automate the fitting. The method we used is explicit an non-iterative.

The 'Jacquelin' method

We will call the method we chose *Jacquelin method*, because we will be referencing an article by J.Jacquelin who developed it for his own purpose **jacquelin**. This method is explicit and non-iterative which is its main advantage. The original derivation presents a universal strategy how to explicitly approximate any function that is a solution to some integral or differential equation. Let us start with derivation of the numerical algorithm for a function:

$$y(x) = a_0 + a_1 e^{b_1 x} + a_2 e^{b_2 x} \quad (2.12)$$

We start by calculating these integrals:

$$\begin{aligned} S(x) &= \int_{x_0}^x y(t) dt \\ &= \int_{x_0}^x a_0 + a_1 e^{b_1 t} + a_2 e^{b_2 t} dt \\ &= a_0(x - x_0) + \frac{a_1}{b_1} (e^{b_1 x} - e^{b_1 x_0}) + \frac{a_2}{b_2} (e^{b_2 x} - e^{b_2 x_0}) \\ \\ SS(x) &= \int_{x_0}^x S(t) dt \\ &= \int_{x_0}^x \int_{x_0}^t y(u) du dt \\ &= \int_{x_0}^x a_0 t + \frac{a_1}{b_1} e^{b_1 t} + \frac{a_2}{b_2} e^{b_2 t} - \left(\frac{a_1}{b_1} e^{a_1 x_0} + \frac{a_2}{b_2} e^{a_2 x_0} + a_0 x_0 \right) dt \\ &= \frac{1}{2} a_0 x^2 - \left(\frac{a_1}{b_1} e^{a_1 x_0} + \frac{a_2}{b_2} e^{a_2 x_0} + a_0 x_0 \right) (x - x_0) - \frac{1}{2} a_0 x_0^2 \\ &\quad + \frac{a_1}{b_1^2} (e^{b_1 x} - e^{b_1 x_0}) + \frac{a_2}{b_2^2} (e^{b_2 x} - e^{b_2 x_0}) \end{aligned}$$

Now, if we reorganize the terms it can be shown that there are constants A , B , C , D and E so that $y(x)$ can be written as:

$$y(x) = A \cdot SS(x) + B \cdot S(x) + Cx^2 + Dx + E. \quad (2.13)$$

By comparing coefficients before the exponential terms e^{b_1x} and e^{b_2x} we get:

$$a_1 = A \frac{a_1}{b_1^2} + B \frac{a_1}{b_1} \quad (2.14)$$

$$a_2 = A \frac{a_2}{b_2^2} + B \frac{a_2}{b_2} \quad (2.15)$$

From that it is possible to see that b_1 and b_2 are roots of the quadratic equation:

$$b^2 - bB - A = 0. \quad (2.16)$$

b_1 and b_2 are then:

$$b_1 = \frac{1}{2} \left(B + \sqrt{B^2 + 4A} \right) \quad (2.17)$$

$$b_2 = \frac{1}{2} \left(B - \sqrt{B^2 + 4A} \right) \quad (2.18)$$

The equation 2.13 is linear in the unknown parameters A, \dots, E and after discretization it can be rewritten as:

$$\mathbf{y} = \mathbf{X} \cdot \mathbf{b} \quad (2.19)$$

where \mathbf{y} is vector:

$$\mathbf{y} = \begin{pmatrix} y_1 \\ y_2 \\ \vdots \\ y_n \end{pmatrix} \quad (2.20)$$

after we set $S_k = S(x_k)$ and $SS_k = SS(x_k)$ we can write:

$$\mathbf{X} = \begin{pmatrix} SS_1 & S_1 & x_1^2 & x_1 & 1 \\ SS_2 & S_2 & x_2^2 & x_2 & 1 \\ SS_3 & S_3 & x_3^2 & x_3 & 1 \\ \vdots & \vdots & \vdots & \vdots & \vdots \\ SS_n & S_n & x_n^2 & x_n & 1 \end{pmatrix} \quad (2.21)$$

and

$$\mathbf{b} = \begin{pmatrix} A \\ B \\ C \\ D \\ E \end{pmatrix} \quad (2.22)$$

and we can use the well-known least squares method to calculate the parameters A, \dots, E . We sort the data so that if $i < j$, then $x_i < x_j$ for $\forall i, j \in \{1, \dots, n\}$. The integrals are computed numerically as:

$$S_i = \begin{cases} 0 & i = 0 \\ S_{i-1} + \frac{1}{2}(y_i + y_{i-1})(x_i - x_{i-1}) & i \in \{2, \dots, n\} \end{cases} \quad (2.23)$$

and

$$SS_i = \begin{cases} 0 & i = 0 \\ SS_{i-1} + \frac{1}{2}(S_i + S_{i-1})(x_i - x_{i-1}) & i \in \{2, \dots, n\} \end{cases} \quad (2.24)$$

Now, the solution to the linear equation 2.19 can be written as **lin-reg**:

$$\mathbf{b} = (\mathbf{X}^T \mathbf{X})^{-1} \cdot (\mathbf{X}^T \mathbf{y}) \quad (2.25)$$

which in our case can be expanded to:

$$\begin{pmatrix} A \\ B \\ C \\ D \\ E \end{pmatrix} = \begin{pmatrix} \sum_{i=1}^n SS_i^2 & \sum_{i=1}^n SS_i S_i & \sum_{i=1}^n SS_i x_i^2 & \sum_{i=1}^n SS_i x_i & \sum_{i=1}^n SS_i \\ \sum_{i=1}^n SS_i S_i & \sum_{i=1}^n S_i^2 & \sum_{i=1}^n S_i x_i^2 & \sum_{i=1}^n S_i x_i & \sum_{i=1}^n S_i \\ \sum_{i=1}^n SS_i x_i^2 & \sum_{i=1}^n S_i x_i^2 & \sum_{i=1}^n x_i^4 & \sum_{i=1}^n x_i^3 & \sum_{i=1}^n x_i^2 \\ \sum_{i=1}^n SS_i x_i & \sum_{i=1}^n S_i x_i & \sum_{i=1}^n x_i^3 & \sum_{i=1}^n x_i^2 & \sum_{i=1}^n x_i \\ \sum_{i=1}^n SS_i & \sum_{i=1}^n S_i & \sum_{i=1}^n x_i^2 & \sum_{i=1}^n x_i & n \end{pmatrix}^{-1} \begin{pmatrix} \sum_{i=1}^n SS_i y_i \\ \sum_{i=1}^n S_i y_i \\ \sum_{i=1}^n x_i^2 y_i \\ \sum_{i=1}^n x_i y_i \\ \sum_{i=1}^n y_i \end{pmatrix} \quad (2.26)$$

After we compute b_1 and b_2 from \mathbf{b} , we still have 3 unknown parameters a_0 , a_1 and a_2 . For those, we will take the original equation 2.12. As it is already linear in the parameters a_0 , a_1 and a_2 , we only need to pre-compute the values of $\alpha_k = e^{b_1 x_k}$ and $\beta_k = e^{b_2 x_k}$. One can see that we get a very similar equation as 2.26, that can be written in this form:

$$\begin{pmatrix} a_0 \\ a_1 \\ a_2 \end{pmatrix} = \begin{pmatrix} n & \sum_{i=1}^n \alpha_i & \sum_{i=1}^n \beta_i \\ \sum_{i=1}^n \alpha_i & \sum_{i=1}^n \alpha_i^2 & \sum_{i=1}^n \alpha_i \beta_i \\ \sum_{i=1}^n \beta_i & \sum_{i=1}^n \alpha_i \beta_i & \sum_{i=1}^n \beta_i^2 \end{pmatrix}^{-1} \begin{pmatrix} \sum_{i=1}^n y_i \\ \sum_{i=1}^n \alpha_i y_i \\ \sum_{i=1}^n \beta_i y_i \end{pmatrix} \quad (2.27)$$

In **jacquelin**, only the case without the constant a_0 is presented, but as we have shown the derivation of the generalized version with constant is not difficult. An extension of Jacquelin method for more than two exponential terms is also not very complicated. Note that adding one term adds two parameters, which leads to matrix of size 7×7 . However, it always leads to solving for the roots of the polynomial created by the first N elements of the vector \mathbf{b} , where N is the number of exponential terms. In case of two exponential terms, equations 2.17 solve for the roots of the polynomial:

$$b^2 - Bb - A = 0 \quad (2.28)$$

In case of three, we would need to calculate $SSS(x)$ from $SS(x)$. There would also be a term x^3 . If we set \mathbf{X} as $[SSS(x), SS(x), S(x), x^3, x^2, x^1, 1]$, we would solve for the roots of:

$$b^3 - Cb^2 - Bb - A = 0. \quad (2.29)$$

Chapter 3

Fitting tool

Chapter 4

Hot electron temperature models

In this chapter, we will talk about the models suitable for hot electron temperature modelling. It was already hinted in the first chapter that there are many physical processes contributing to the absorption of laser. As a consequence, there is a non-linear relationship between the initial parameters and the hot electron temperature. It would be very difficult to propose an analytical model where the temperature is explicitly dependant on all the initial parameters. There have been works studying how the temperature scales with respect to intensity [2], [7], [11], [13], [17], angle [7] or length scale and even pulse durations [17] but none of them model all parameters

Chapter 5

Hot electron temperature modelling

Chapter 6

Comparison to contemporary data

Conclusion

Bibliography

- [1] T. D. Arber, K. Bennett, C. S. Brady, *et al.*, “Contemporary particle-in-cell approach to laser-plasma modelling”, *Plasma Physics and Controlled Fusion*, vol. 57, 11 Sep. 2015, ISSN: 13616587. DOI: 10.1088/0741-3335/57/11/113001.
- [2] F. N. Beg, A. R. Bell, A. E. Dangor, *et al.*, “A study of picosecond laser–solid interactions up to 1019 wcm²”, *Physics of Plasmas*, vol. 4, pp. 447–457, 2 Feb. 1997, ISSN: 1070-664X. DOI: 10.1063/1.872103.
- [3] C. K. Birdsall and A. B. Langdon, *Plasma physics via computer simulation*. McGraw-Hill, 1985, ISBN: 0070053715.
- [4] F. Brunel, “Not-so-resonant, resonant absorption”, *Physical Review Letters*, vol. 59, pp. 52–55, 1 Jul. 1987, ISSN: 0031-9007. DOI: 10.1103/PhysRevLett.59.52.
- [5] H.-b. Cai, W. Yu, S.-p. Zhu, and C.-y. Zheng, “Short-pulse laser absorption via $j \times b$ heating in ultrahigh intensity laser plasma interaction”, *Physics of Plasmas*, vol. 13, 11 Nov. 2006, ISSN: 1070-664X. DOI: 10.1063/1.2372463.
- [6] F. F. Chen, *Introduction to plasma physics and controlled fusion*. Plenum Press, 1984, ISBN: 0306413329.
- [7] Y. Q. Cui, W. M. Wang, Z. M. Sheng, Y. T. Li, and J. Zhang, “Laser absorption and hot electron temperature scalings in laser-plasma interactions”, *Plasma Physics and Controlled Fusion*, vol. 55, 8 Aug. 2013. DOI: 10.1088/0741-3335/55/8/085008.
- [8] J. Dawson, “One-dimensional plasma model”, *Physics of Fluids*, vol. 5, pp. 445–459, 4 1962. DOI: 10.1063/1.1706638.
- [9] T. Esirkepov, “Exact charge conservation scheme for particle-in-cell simulation with an arbitrary form-factor”, *Computer Physics Communications*, vol. 135, pp. 144–153, 2001. DOI: 10.1016/S0010-4655(00)00228-9. [Online]. Available: www.elsevier.nl/locate/cpc.
- [10] P. Gibbon, “Introduction to plasma physics”, CERN, 2014, pp. 51–65, ISBN: 9789290834250. DOI: 10.5170/CERN-2016-001.51.
- [11] M. G. Haines, M. S. Wei, F. N. Beg, and R. B. Stephens, “Hot-electron temperature and laser-light absorption in fast ignition”, *Physical Review Letters*, vol. 102, p. 045008, 4 Jan. 2009, ISSN: 0031-9007. DOI: 10.1103/PhysRevLett.102.045008.

- [12] C. J. Joachain, N. J. Kylstra, and R. M. Potvliege, *Atoms in Intense Laser Fields*. Cambridge University Press, Dec. 2011, ISBN: 9780521793018. DOI: 10.1017/CB09780521793018.
- [13] T. Kluge, T. Cowan, A. Debus, U. Schramm, K. Zeil, and M. Bussmann, “Electron temperature scaling in laser interaction with solids”, *Physical Review Letters*, vol. 107, p. 205003, 20 Nov. 2011, ISSN: 0031-9007. DOI: 10.1103/PhysRevLett.107.205003.
- [14] W. L. Kruer, *The Physics Of Laser Plasma Interactions*. CRC Press, Aug. 2019, ISBN: 9781003003243. DOI: 10.1201/9781003003243.
- [15] A. Macchi, *A Superintense Laser-Plasma Interaction Theory Primer*, 1st ed. Springer Dordrecht, 2013, ISBN: 978-94-007-6124-7. DOI: 10.1007/978-94-007-6125-4. [Online]. Available: <http://www.springer.com/series/8902>.
- [16] P. Michel, *Introduction to Laser-Plasma Interactions*. Springer International Publishing, 2023, ISBN: 978-3-031-23423-1. DOI: 10.1007/978-3-031-23424-8.
- [17] K. G. Miller, D. R. Rusby, A. J. Kemp, S. C. Wilks, and W. B. Mori, “Maximizing mev x-ray dose in relativistic laser-solid interactions”, *Physical Review Research*, vol. 5, p. L012044, 1 Mar. 2023, ISSN: 2643-1564. DOI: 10.1103/PhysRevResearch.5.L012044.
- [18] T. Pfeifer, C. Spielmann, and G. Gerber, “Femtosecond x-ray science”, *Reports on Progress in Physics*, vol. 69, pp. 443–505, 2 Feb. 2006, ISSN: 0034-4885. DOI: 10.1088/0034-4885/69/2/R04.
- [19] C. Reich, P. Gibbon, I. Uschmann, and E. Förster, “Yield optimization and time structure of femtosecond laser plasma k-alpha sources”, *Physical Review Letters*, vol. 84, pp. 4846–4849, 21 May 2000, ISSN: 0031-9007. DOI: 10.1103/PhysRevLett.84.4846.
- [20] F. Ricardo, “Computational challenges in laser-plasma interactions”, in D. A. Jaroszynski, R. Bingham, and R. Cairns, Eds. CRC Press, Mar. 2009, ISBN: 9780429146954. DOI: 10.1201/9781584887799.
- [21] H. Schwöerer, “Generation of x-rays by intense femtosecond lasers”, in Sep. 2004, pp. 235–254. DOI: 10.1007/978-3-540-39848-6_17.
- [22] Z.-M. Sheng, S.-M. Weng, L.-L. Yu, *et al.*, “Absorption of ultrashort intense lasers in laser–solid interactions”, *Chinese Physics B*, vol. 24, 1 Jan. 2015, ISSN: 1674-1056. DOI: 10.1088/1674-1056/24/1/015201.
- [23] H. Takabe, *The Physics of Laser Plasmas and Applications - Volume 1*. Springer, 2020. [Online]. Available: <http://www.springer.com/series/15614>.
- [24] D. Tskhakaya, K. Matyash, R. Schneider, and F. Taccogna, “The particle-in-cell method”, *Contributions to Plasma Physics*, vol. 47, pp. 563–594, 8-9 2007. DOI: 10.1002/ctpp.200710072.
- [25] J. Wang, Z. Chen, Y. Wang, *et al.*, “Three-dimensional parallel unipic-3d code for simulations of high-power microwave devices”, *Physics of Plasmas*, vol. 17, 7 Jul. 2010, ISSN: 1070664X. DOI: 10.1063/1.3454766.

- [26] S. Wilks and W. Kruer, “Absorption of ultrashort, ultra-intense laser light by solids and overdense plasmas”, *IEEE Journal of Quantum Electronics*, vol. 33, pp. 1954–1968, 11 1997, issn: 00189197. DOI: 10.1109/3.641310.
- [27] V. Yanovsky, V. Chvykov, G. Kalinchenko, *et al.*, “Ultra-high intensity- 300-tw laser at 0.1 hz repetition rate”, *Optics Express*, vol. 16, p. 2109, 3 2008, issn: 1094-4087. DOI: 10.1364/OE.16.002109.
- [28] K. S. Yee, “Numerical solution of initial boundary value problems involving maxwell’s equations in isotropic media”, *IEEE Transactions on Antennas and Propagation*, vol. 14, pp. 302–307, 3 May 1966. DOI: 10.1109/TAP.1966.1138693.

Appendix A

Attachment

Attachment